# Electrocatalytic Reduction of Carbon Dioxide to Methane on Single Transition Metal Atoms Supported on a Defective Boron Nitride Monolayer: First Principle Study

*Xin Tan,* Hassan A. Tahini, Hamidreza Arandiyan, and Sean C. Smith**

**The electrochemical conversion of carbon dioxide ($CO_2$) and water into useful multi-electron transfer products, such as methanol ($CH_3OH$) and methane ($CH_4$), is a major challenge in facilitating a closed carbon cycle. Here, a systematic first principle study of the potential of single transition metal atoms (Sc to Zn, Mo, Rh, Ru, Pd, Ag, Pt, and Au) supported on experimentally available defective boron nitride monolayers with a boron monovacancy (TM/defective BN) to achieve highly efficient electrocatalytic $CO_2$ reduction (ECR) to $CH_4$ is carried out. Our computations reveal that Fe/defective BN, Co/defective BN, and Pt/defective BN nanosheets possess outstanding ECR activities with quite low (less negative) onset potentials of −0.52, −0.68, and −0.60 V, respectively. Given that Fe and Co are nonprecious metals, Fe/defective BN and Co/defective BN may provide cost-effective electrocatalysts. The high ECR activities of these TM/defective BN catalyst systems stem from the moderate electrocatalysts' affinities for C and O, which modulate the free energies of ECR intermediates in the reaction pathways. Moreover, it is found that Fe/defective BN and Pt/defective BN show high selectivity of ECR to $CH_4$. This finding highlights a strategy to design highly active and selective single-atom electrocatalysts for ECR to $CH_4$.**

## 1. Introduction

Utilization of carbon dioxide ($CO_2$) as a carbon source to synthesize valuable chemicals has the potential to mitigate the greenhouse effect while generate high-energy density fuels and other commodities.[1,2] Due to $CO_2$'s inherent thermodynamic stability and chemical inertness, the activation of $CO_2$ and its subsequent hydrogenation to hydrocarbons is challenging.[3] Electrocatalytic $CO_2$ reduction (ECR) to chemical fuels or other useful chemicals, using only water, $CO_2$, and electricity as inputs, has attracted considerable attention as a promising process because of its straightforward operation in comparison to high-temperature reactors.[4–10] According to the number of transferred electrons and protons in the ECR, a wide variety of product channels is in principle accessible, including the two-electron products carbon monoxide (CO), formaldehyde (HCHO), and formic acid (HCOOH); the six-electron product methanol ($CH_3OH$); and the complete eight-electron product methane ($CH_4$);[11–14] not to mention the competitive hydrogen evolution reaction (HER). This promising technique is hampered by the lack of efficient ECR electrocatalysts that are capable of reducing $CO_2$ beyond the two-electron products, such as $CH_3OH$ and $CH_4$, with $CH_4$ being one of the simplest hydrocarbons and a primary component of natural gas with an existing infrastructure for storage, distribution, and consumption.[15–18]

Although many heterogeneous and homogeneous electrocatalysts have been screened for their effectiveness in the ECR to multi-electron transfer products in both experiments and computations for many decades, the availability of efficient electrocatalysts is still very limited. Pure metallic Cu is the only transition metal (TM) that selectively promotes ECR to hydrocarbons, predominantly $CH_4$, with significant quantities (faradaic efficiency ≈72.3%) at high current densities (≈5 mA $cm^{-2}$).[19–23] However, the ECR on Cu requires a prohibitively high overpotential (on the order of 1 V), making Cu an inefficient electrocatalyst for the ECR. Well-dispersed Cu nanoparticles supported on glassy carbon have been successfully prepared, which show enhanced electrochemical methanation of $CO_2$ comparable to those of much more expensive Cu single-crystal electrodes.[15] Both experimental and theoretical analysis have suggested that $Mo_2C$ electrocatalysts are capable of ECR into $CH_4$ fuel at low onset potential (≈−0.55 V), while an acceleration of the competitive HER was also observed in the presence of $CO_2$.[24,25] In addition, Li et al. has predicted from density functional theory (DFT) calculations that the $Cr_3C_2$ and $Mo_3C_2$ MXenes exhibit promising $CO_2$ to $CH_4$ selective conversion capabilities.[26]

Dr. X. Tan, Dr. H. A. Tahini, Prof. S. C. Smith
Integrated Materials Design Laboratory
Department of Applied Mathematics
Research School of Physics and Engineering
The Australian National University
Canberra, ACT 2601, Australia
E-mail: Xin.Tan@anu.edu.au; Sean.Smith@anu.edu.au
Dr. H. Arandiyan
Laboratory of Advanced Catalysis for Sustainability
School of Chemistry
The University of Sydney
Sydney, NSW 2006, Australia

DOI: 10.1002/adts.201800094

Recent DFT and experimental results have shown that the use of graphitic carbon nitride ($g$-$C_3N_4$) as a molecular scaffold to coordinate the active Cu centers (Cu–$C_3N_4$ complex) presents a new molecular-level strategy for the development of electrocatalysts with high ECR selectivity toward hydrocarbon/alcohol.[27] Clearly, both theoretical and experimental investigations are proving important to develop high-performance electrocatalysts for the ECR to multi-electron transfer products.

Single-atom catalysts (SACs), in which single metal atoms anchored to supports, have recently emerged as a new research frontier in the catalysis community.[28–33] With uniform single-atom dispersion and well-defined configuration, SACs not only represent the cost-effective utilization of precious metallic catalysts, but also open up considerable new territory for optimizing selectivity and activity for various reactions. Very recently, DFT calculations have been performed to systematically study the possibility of a series of single TM atoms supported on the experimentally available defective boron nitride monolayer with a boron monovacancy (TM/defective BN) as nitrogen fixation electrocatalysts.[34] The results revealed that Mo/defective BN nanosheets are very stable and possess outstanding nitrogen fixation electrocatalytic activity, which opens a new avenue of ammonia production by SACs under ambient conditions.

In this work, we use first principle DFT computations to systematically investigate the potential of TM/defective BN (TM = Sc to Zn, Mo, Rh, Ru, Pd, Ag, Pt, and Au) as highly efficient electrocatalysts for ECR to $CH_4$. Our DFT results demonstrate that Fe/defective BN, Co/defective BN, and Pt/defective BN possess outstanding ECR activities with quite low (less negative) onset potentials of −0.52, −0.68, and −0.60 V, respectively, which are less negative than other ECR electrocatalysts, such as Cu (100) (−0.78 V), Cu (211), (−0.67 V), and Cu–$C_3N_4$ complex (−0.75 V). Given that Fe and Co are nonprecious metals, Fe/defective BN and Co/defective BN are cost-effective electrocatalysts. The high ECR activities of those TM/defective BN stem from moderate electrocatalysts' affinities for C and O, which modulate the free energies of ECR intermediates in the reaction pathways. Moreover, we also find that Fe/defective BN and Pt/defective BN show high selectivity of ECR to $CH_4$. These findings clarify the ECR mechanism on TM/defective BN and offer a strategy to design highly active and selective single-atom electrocatalysts for ECR to $CH_4$.

## 2. Results and Discussion

### 2.1. $CO_2$ Adsorption on Various TM/defective BN Nanosheets

Given that chemisorption of $CO_2$ on electrocatalysts is the first step that occurs during the ECR, which guarantee sufficient activation of the inert $CO_2$ molecule, we first study the $CO_2$ adsorption on a series of 3*d*, 4*d*, and 5*d* TM atoms (TM = Sc ∼ Zn, Mo, Rh, Ru, Pd, Ag, Pt, and Au) supported by a defective BN nanosheet. Here, we consider two $CO_2$ adsorption configurations: the $CO_2$ may interact with TM/defective BN either through physisorption, where $CO_2$ is attached to the surface through a noncovalent interaction between the O atom of $CO_2$ and the TM atom (Figure 5b), or through chemisorption, in which the C atom of $CO_2$ is formally bound with the TM atom (Figure 5c). To determine the thermodynamic stability of $CO_2$ on TM/defective BN, we calculate the adsorption energy ($E_{ads}$) of $CO_2$, which defined as $E_{ads} = E_{CO_2+TM/BN} - E_{TM/BN} - E_{CO_2}$, where $E_{CO_2+TM/BN}$, $E_{TM/BN}$, and $E_{CO_2}$ represent the total energy of the TM/defective BN with adsorbed $CO_2$, the bare TM/defective BN, and the isolated $CO_2$ molecule, respectively. Figure 5d shows the $E_{ads}$ of $CO_2$ on various TM/defective BN. On Sc, Ni, Cu, Zn, Pd, Ag, and Au atoms supported by a defective BN, $CO_2$ is only physisorbed on the electrocataysts, suggesting that those nanosheets are inappropriate as ECR electrocatalysts due to their poor performance for $CO_2$ activation. On the other hand, $CO_2$ is both physisorbed and chemisorbed on other 10 atoms (including Ti ∼ Co, Mo, Ru, Rh, and Pt) supported by a defective BN. Furthermore, those nanosheets seem to be active toward $CO_2$ chemisorption, exhibiting spontaneous adsorption energies between −1.25 and −0.14 eV. Those TM/defective BN nanosheets that are seen to facilitate the chemisorption of $CO_2$ molecule are potential electrocatalysts for the ECR, hence, we will focus on the TM/defective BN (TM = Ti ∼ Co, Mo, Ru, Rh, and Pt) systems in the following discussions.

### 2.2. Screening TM/defective BN Nanosheets as ECR Electrocatalysts

To investigate the process of ECR to $CH_4$ on TM/defective BN, we consider different reaction pathways in this work, as depicted in **Figure 1**a, that have been proposed as possible reaction pathways for ECR to $CH_4$ in previous investigations.[18,21,23,27] By calculating the free energies of adsorbed intermediates along the reaction pathways, we obtain the free energy diagram and the onset potential, $U_{onset}$, for ECR to $CH_4$ on various TM/defective BN, as shown in Figure 1b. The onset potentials on Fe/defective BN, Co/defective BN, and Pt/defective BN are −0.52, −0.68, and −0.60 V, respectively, which are less negative than those on Cu (100) (−0.78 V),[23] Cu (211) (−0.67 V),[23,25] and Cu–$C_3N_4$ complex (−0.75 V)[27]. We also note that these values are comparable to those on other electrocatalysts with single transition atom or transition metal dimers for ECR to $CH_4$, such as Pt@dv−Gr (−0.52 V),[35] cobalt–porphyrin nanotubes (−0.58 V),[36] transition metal dimers supported on graphene (−0.61∼−0.70 V),[37] and Cu-terminated armchair graphene nanoribbons (−0.44∼−0.58 V).[38] These results suggest that the Fe, Co, and Pt TM/defective BN nanosheet systems are excellent potential electrocatalyst materials for ECR to $CH_4$. It is noteworthy that Fe and Co are nonprecious metals, therefore, Fe/defective BN and Co/defective BN appear to offer the most cost-effective electrocatalysts for ECR to $CH_4$.

### 2.3. The Electrocatalytic Mechanism of ECR on Fe/defective BN, Co/defective BN, and Pt/defective BN Nanosheets

In order to study the electrocatalytic mechanism of ECR on Fe/defective BN, Co/defective BN, and Pt/defective BN, we calculate the free energy diagrams of ECR to $CH_4$ through different reduction pathways. **Figure 2**b–d show the free energy diagrams of ECR to $CH_4$ on Fe/defective BN, Co/defective BN, and

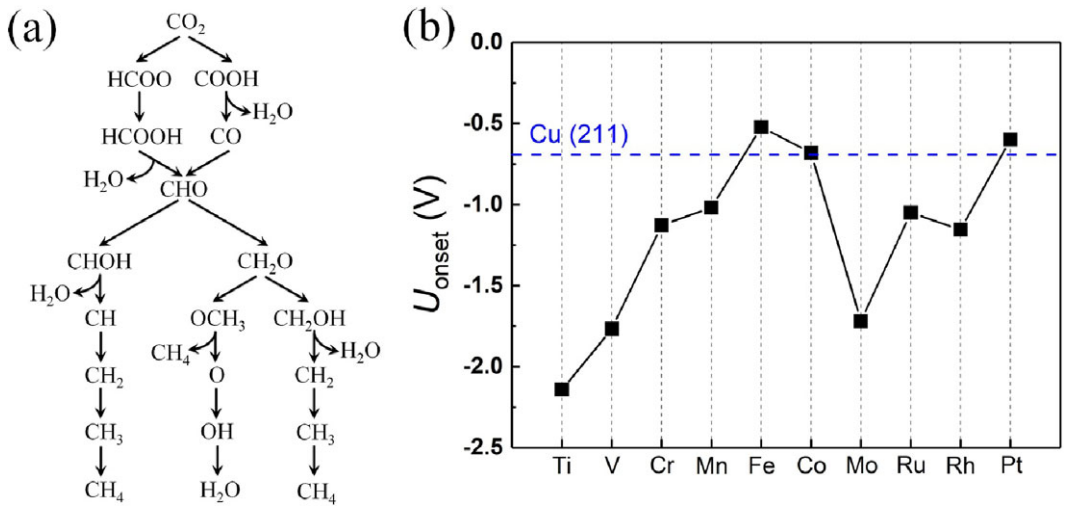


**Figure 1.** a) Different possible reaction pathways for ECR to $CH_4$ according to previous investigations. b) The onset potentials for ECR to $CH_4$ on various TM/defective BN nanosheets. The blue dashed line denotes the onset potential for ECR to $CH_4$ on Cu (211) surface.

Pt/defective BN, respectively. Clearly, the minimum energy pathways for ECR to $CH_4$ on those nanosheets are the same, following $CO_2 \rightarrow *COOH \rightarrow *CO \rightarrow *CH_2O \rightarrow *OCH_3 \rightarrow *O \rightarrow *OH \rightarrow H_2O$ (the corresponding absorbed intermediate configurations on Fe/defective BN are shown in Figure 2a, which are consistent with those on the (111), (100), and (211) facets of Cu crystal.[23,25] The absorbed intermediate configurations on Co/defective BN and Pt/defective BN are similar to those on Fe/defective BN (data not shown here). On Fe/defective BN, the rate-limiting step is the proton/electron-transfer step of *OH (i.e., $*OH \rightarrow H_2O$), with an energy barrier of 0.52 eV, while the rate-limiting steps on Co/defective BN and Pt/defective BN lie in the protonation step of *CO (i.e., $*CO \rightarrow *CHO$), with energy barriers of 0.68 and 0.60 eV, respectively. The results are also similar to those on the (111), (100), and (211) facets of Cu crystal that the rate-limiting step of ECR to $CH_4$ is either $*OH \rightarrow H_2O$ or $*CO \rightarrow *CHO$ reaction.[23,25]

### 2.4. The Origin of High ECR Activity on Fe/defective BN, Co/defective BN, and Pt/defective BN Nanosheets

Insights into the origin of high ECR activity on TM/defective BN nanosheets can guide the design of better electrocatalysts. In Nørskov's method, the limiting potential for each electrochemical step, $U_L$, at which the electrochemical step of a reaction becomes exergonic (or downhill in free energy), is determined by the free energies of adsorbed intermediates.[19] In other words, the diverse ECR performance stems from different binding strengths of the adsorbed intermediates on different electrocatalysts. Therefore, it is crucial to identify the relationship between the free energies of adsorbed intermediates and electrocatalytic activity for rational search of more-effective electrocatalysts. Previous works[23,25] have found that there are seven adsorbed intermediates along the minimum energy pathway for ECR to $CH_4$ on the (111), (100), and (211) facets of Cu crystal. The first half of the intermediates, that is, *COOH, *CO, *CHO, and $*CH_2O$, interact with the electrocatalyst surface through a C atom, and the second half, that is, $*OCH_3$, *O, and *OH, interact through an O atom. The $U_L$ for each elementary step can be estimated as a function of the electrocatalysts' C or O affinity. Given that the minimum energy pathways for ECR to $CH_4$ on TM/defective BN are the same as those on Cu crystal, we can correlate ECR activity on TM/defective BN as a function of the electrocatalysts' affinity for C and O. Here we use the free energies of *COOH and *OH to represent the electrocatalysts' affinities for C and O, respectively.

**Figure 3** shows the $U_L$ for the two possible rate-limiting steps, that is, $*OH \rightarrow H_2O$ and $*CO \rightarrow *CHO$ reactions, on TM/defective BN as a function of the free energies of *OH and *COOH, respectively. The results show that the binding strengths both of *OH and *COOH on TM/defective BN decrease as we move along the row of periodic table of elements, indicating that the TM/defective BN which binds carbon also strongly binds oxygen strongly. Moreover, the $U_L$ for $*OH \rightarrow H_2O$ reaction becomes less negative as the electrocatalysts' affinity for O (*OH) decrease. On the contrary, with the decrease of the electrocatalysts' affinity for C (*COOH), the $U_L$ for $*CO \rightarrow *CHO$ reaction become more negative. By comparing the $U_L$ for $*OH \rightarrow H_2O$ and $*CO \rightarrow *CHO$, we find that the $U_L$ for $*CO \rightarrow *CHO$ reaction is much less negative; it is only for electrocatalysts that have low affinities for both O (*OH) and C (*COOH), such as Co/defective BN and Rh/defective BN, the limitations set by the $*CO \rightarrow *CHO$ reaction becomes comparable or exceeded to the potential of clearing *OH from the surface. This does indicate that for most TM/defective BN, $*OH \rightarrow H_2O$ reaction is the rate-limiting step, and *OH removal will likely limit the electrocatalysts' effectiveness due to the strong *OH binding (more negative $\Delta G(*OH)$), however, for TM/defective BN with their low C and O affinity, the rate-limiting step will be set by the $CO* \rightarrow CHO*$ reaction. Thus, high ECR activity TM/defective BN should have the optimal (moderate) values of electrocatalysts' C and O affinity. As shown in Figure 3, Fe/defective BN, Co/defective BN, and Pt/defective BN nanosheets have moderate affinities for C and O, that is the reason why those electrocatalysts have high activity for ECR to $CH_4$.

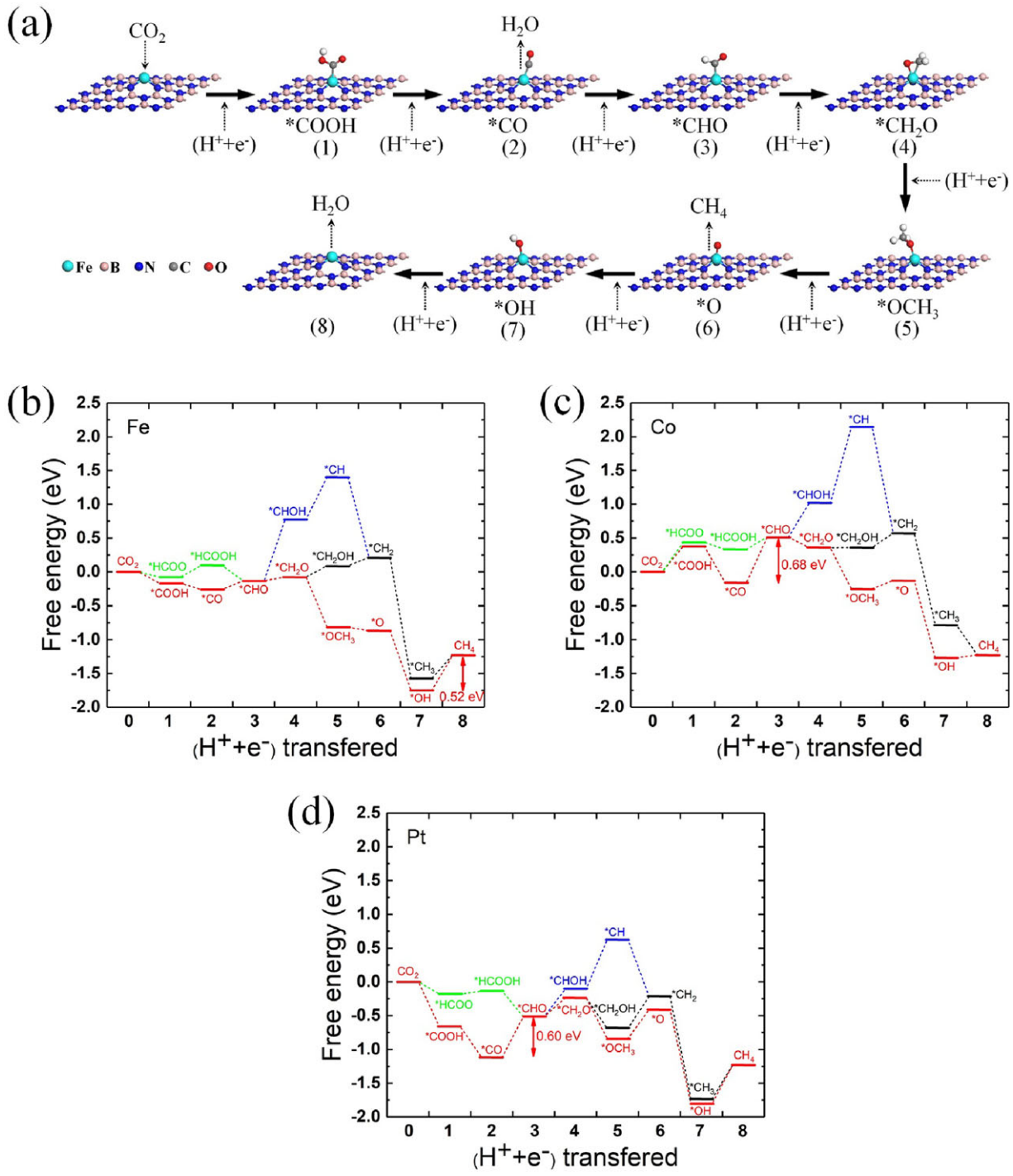


**Figure 2.** a) The adsorbed intermediate configurations along the minimum energy pathway for ECR to $CH_4$ on Fe/defective BN nanosheet. The free energy diagrams of ECR to $CH_4$ on b) Fe/defective BN, c) Co/defective BN, and d) Pt/defective BN. The red arrows denote the rate-limiting steps.

### 2.5. The Selectivity of ECR to $CH_4$ on Fe/defective BN, Co/defective BN, and Pt/defective BN Nanosheets

Selectivity is an important parameter for highly efficient electrocatalysts. Because of the complexity of ECR, the electrocatalysts can reduce $CO_2$ to several products, including the two-electron products CO and HCOOH, the six-electron product $CH_3OH$, and the complete eight-electron product $CH_4$.[11–14] In addition, HER can be a dominant side reaction that is competitive with the ECR path.[12,18,25] An effective ECR electrocatalyst should thus show poor activity for the competitive HER.

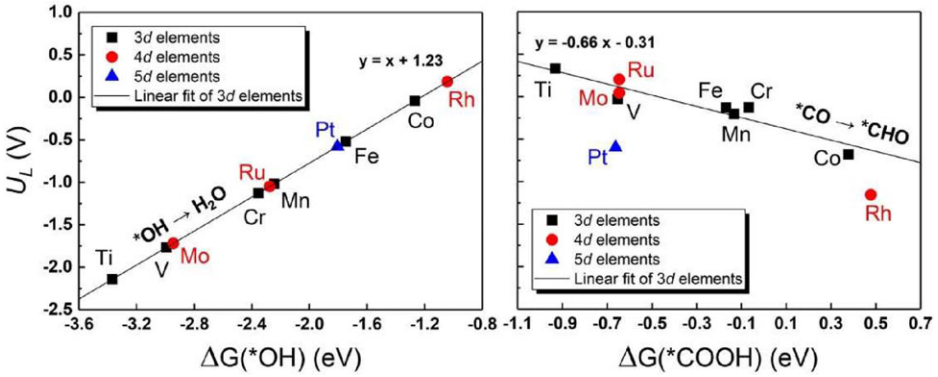


**Figure 3.** The $U_L$ for two possible rate-limiting steps, that is, *OH → $H_2O$ (left) and *CO → *CHO (right) reactions, on TM/defective BN nanosheets as a function of the free energies of *OH and *COOH, respectively.

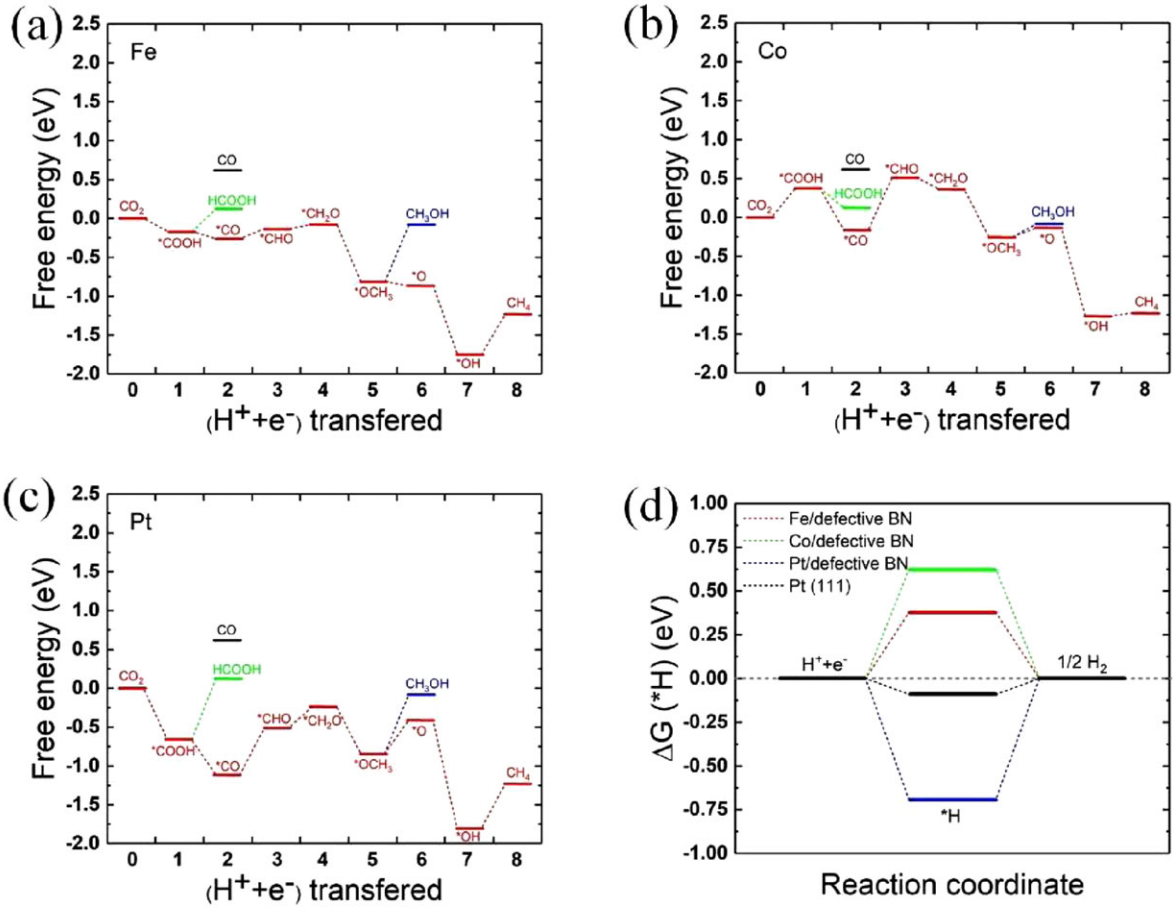


**Figure 4.** The free energy diagrams of ECR toward the production of HCOOH, CO, and $CH_3OH$ in comparison with that for $CO_2$ methanation on a) Fe/defective BN, b) Co/defective BN, and c) Pt/defective BN nanosheets, respectively. Here, only the minimum energy pathway is shown. d) The free energy diagram of HER for Fe/defective BN, Co/defective BN, and Pt/defective BN nanosheets. The free energy diagram of HER for Pt (111) is also shown for comparison.

In order to investigate the selectivity of ECR to $CH_4$ on Fe/defective BN, Co/defective BN, and Pt/defective BN nanosheets, the minimum energy pathways toward the production of HCOOH, CO, and $CH_3OH$ are examined in comparison with the minimum energy pathway for $CO_2$ methanation on those nanosheets, as shown in **Figure 4**a–c. In general, the reaction pathways and the free energy diagrams of ECR toward HCOOH, CO, $CH_3OH$, and $CH_4$ on Fe/defective BN (Figure 4a) and Pt/defective BN (Figure 4c) display similar trends, hence here we use Fe/defective BN as an example to explain the selectivity of ECR to $CH_4$ on those two nanosheets. On Fe/defective BN (Figure 4a), the dissociation of *COOH to form *CO is

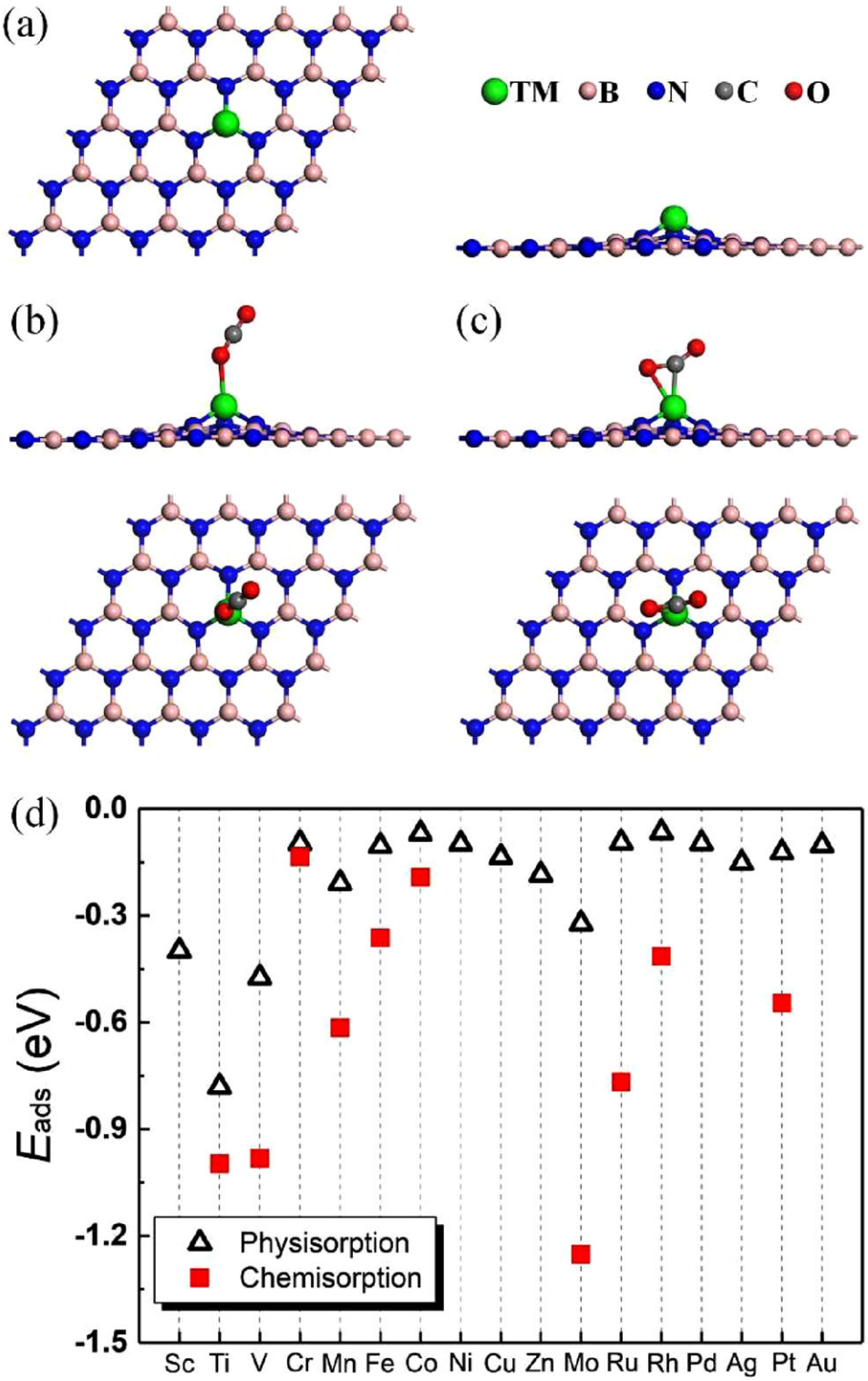


**Figure 5.** a) Top (left) and side (right) views of a TM/defective BN (TM = Sc ~ Zn, Mo, Rh, Ru, Pd, Ag, Pt, and Au) nanosheet. Optimized structures of $CO_2$ b) physisorption and c) chemisorption on TM/defective BN. d) The $E_{ads}$ of a $CO_2$ on various TM/defective BN.

**Table 1.** Contribution to the free energies of adsorbed intermediates and non-adsorbed gas-phase molecules from ZPE correction, enthalpic temperature correction, and entropy contribution. All are given in eV.

| Species | ZPE | $\int C_P dT$ | $-TS$ |
|---|---|---|---|
| *COOH | 0.62 | 0.10 | −0.18 |
| *HCOO | 0.62 | 0.10 | −0.23 |
| *CO | 0.19 | 0.07 | −0.15 |
| *CHO | 0.44 | 0.09 | −0.18 |
| *$CH_2O$ | 0.76 | 0.09 | −0.19 |
| *$OCH_3$ | 1.11 | 0.09 | −0.18 |
| *O | 0.07 | 0.03 | −0.04 |
| *OH | 0.36 | 0.05 | −0.08 |
| *H | 0.16 | 0.01 | −0.01 |
| $CO_2$ | 0.31 | 0.10 | −0.65 |
| CO | 0.14 | 0.09 | −0.67 |
| $H_2$ | 0.27 | 0.09 | −0.42 |
| $H_2O$ | 0.58 | 0.10 | −0.65 |
| HCOOH | 0.90 | 0.11 | −1.02 |
| $CH_3OH$ | 1.35 | 0.11 | −0.79 |
| $CH_4$ | 1.20 | 0.10 | −0.60 |

exothermic during the formation of $CH_4$ (red line), while the hydrogenation of *COOH to give HCOOH possesses a barrier of 0.29 eV (green line), suggesting that the formation of HCOOH is unfavorable for the ECR on Fe/defective BN. The desorption of CO possesses a large barrier of 0.88 eV (black line), which is much higher than that of the hydrogenation of *CO to *CHO (0.13 eV) during the formation of $CH_4$ (red line), indicating that the formation of CO is also unfavorable for the ECR on Fe/defective BN. The barrier for the hydrogenation of *$OCH_3$ to form $CH_3OH$ is 0.73 eV (blue line); however, the dissociation of *$OCH_3$ into *O is exothermic during the formation of $CH_4$ (red line), which means that the formation of $CH_4$ is more favorable than $CH_3OH$ production on Fe/defective BN. In a word, all these results show high selectivity of $CH_4$ on Fe/defective BN and Pt/defective BN nanosheets during the ECR to $CH_4$. However, the case is different on Co/defective BN (Figure 4b), the free energy of *CHO (red line) is 0.39 eV higher than that of HCOOH (green line), and the barrier for the dissociation of *$OCH_3$ into *O (red line) is only 0.05 eV lower than that for the hydrogenation of *$OCH_3$ to form $CH_3OH$ (blue line). These results indicate that the selectivity of $CH_4$ from HCOOH and $CH_3OH$ on Co/defective BN is not as good as that on Fe/defective BN and Pt/defective BN.

We also calculate the free energy diagram of HER for Fe/defective BN, Co/defective BN, and Pt/defective BN nanosheets, as shown in Figure 4d. The overall HER mechanism can be evaluated with a three-state diagram consisting of an initial $H^+$ state, an intermediate *H state, and 1/2 $H_2$ as the final product.[39] The $\Delta G$(*H) is proven to be a key descriptor to characterize the HER activity of electrocatalyst. The optimum value of $|\Delta G(*H)|$ should be zero; for instance, this value for the well-known highly efficient Pt (111) electrocatalyst is near-zero as $|\Delta G(*H)| \approx 0.09$ eV.[39] Clearly, in terms of the selectivity of $H_2$ gas production, Fe/defective BN, Co/defective BN, and Pt/defective BN nanosheets show poor activities for HER with $\Delta G(*H) = 0.38$, 0.62, and −0.69 eV, respectively, implying that HER is unlikely to interfere as an unwanted competitive pathway to the ECR.

## 3. Conclusions

In summary, we have carried out a comprehensive study of the potential of single transition metal atoms (Sc to Zn, Mo, Rh, Ru, Pd, Ag, Pt, and Au) supported on the experimentally available defective boron nitride monolayer with a boron monovacancy as an effective electrocatalyst for ECR to $CH_4$, by means of DFT computations. We found that Fe/defective BN, Co/defective BN, and Pt/defective BN possess outstanding electrocatalytic activities for ECR to $CH_4$ with quite low onset potentials of −0.52, −0.68, and −0.60 V, respectively, which are less negative than other ECR electrocatalysts, such as Cu (100) (−0.78 V), Cu (211) (−0.67 V), and Cu–$C_3N_4$ complex (−0.75 V). Given that Fe and Co are nonprecious metals, Fe/defective BN and Co/defective BN are cost-effective electrocatalysts. The high ECR activities of those TM/defective BN stem from the moderate electrocatalysts' affinities for C and O, which modulate the free energies of ECR intermediates in the reaction pathways. Comparing the free energy diagrams of HER and ECR toward HCOOH, CO, $CH_3OH$, and $CH_4$ on those TM/defective, we also found that Fe/defective BN and Pt/defective BN show high selectivity of ECR toward $CH_4$. This finding not only clarifies the ECR mechanism on TM/defective BN nanosheets, but also offers a strategy to design highly active and selective SACs, including nonprecious Fe/defective BN and precious Pt/defective BN, for ECR to $CH_4$.

## 4. Experimental Section

All of the spin-polarized DFT calculations were performed using the VASP program,[40–42] which uses a plane-wave basis set and a projector-augmented wave (PAW) method for the treatment of core electrons.[43] The Perdew, Burke, and Ernzerhof exchange-correlation functional within a generalized gradient approximation (GGA-PBE)[44] was used in the calculations, and the van der Waals (vdW) correction proposed by Grimme (DFT-D2)[45] was employed due to its good description of long-range vdW interactions. For the expansion of wavefunctions over the plane-wave basis set, a converged cutoff was set to 450 eV.

In order to simulate the defective BN monolayer with a boron monovacancy, a 5 × 5 BN supercell with periodical boundary conditions was used, and then, one B atom was removed to create a boron monovacancy, which provides an anchoring site for a single TM atom (**Figure 5**a). The vacuum space was set to larger than 18 Å in the *z* direction to avoid interactions between periodic images. In geometry optimizations, all the atomic coordinates were fully relaxed up to the residual atomic forces smaller than 0.005 eV $Å^{-1}$, and the total energy was converged to $10^{-5}$ eV. The Brillouin zone integration was performed on the (4 × 4 × 1) Monkhorst–Pack k-point mesh.[46]

Eight net coupled proton and electron transfer steps are involved in ECR to $CH_4$ process ($CO_2 + 8H^+ + 8e^- \rightarrow CH_4 + 2H_2O$). Each ECR step involves the transfer of a proton coupled with an electron from solution to an adsorbed intermediate on the surface of electrocatalysts. The free energies of the adsorbed intermediates in reaction pathways were calculated based on a computational hydrogen electrode (CHE) model proposed by Nørskov et al.[21,23]. In this model, the free energy changes at each electrochemical step involving an proton-electron transfer are calculated using the definition that the free energy of ($H^+ + e^-$) equals to $\frac{1}{2}H_2(g)$ for

standard hydrogen electrode (SHE). According to this method, the free energy change of the reaction, $\Delta G$, was calculated as the difference between the free energies of initial and final states as[21,23]

$$\Delta G = \Delta E + \Delta \mathrm{ZPE} + \Delta \int C_p \mathrm{d}T - T\Delta S \quad (1)$$

where $\Delta E$ corresponds to the total energy change directly obtained from DFT calculations, ZPE is the zero-point energy, $C_p$ is the heat capacity, $T$ is temperature, and $S$ is the entropy. Here, zero-point energies, heat capacities, and entropies of adsorbed intermediates and non-adsorbed gas-phase molecules were adopted from the previous literature, as listed in **Table 1**.[21,23] The adsorbate solvation effects were included approximately in the same manner as in the previous studies: adsorbates *OH, *R–OH, *CHO, and *CO are stabilized by −0.5, −0.25, −0.1, and −0.1 eV, respectively.[21,23]

## Acknowledgements

S.S. and H.A. acknowledge the financial support by the Australian Research Council under Discovery Project (DP170104853). This research was undertaken with the assistance of resources provided by the National Computing Infrastructure facility at the Australian National University, allocated through both the National Computational Merit Allocation Scheme supported by the Australian Government and the Australian Research Council grant LE120100181 (Enhanced merit-based access and support at the new NCI petascale supercomputing facility, 2012–2015).

## Conflict of Interest

The authors declare no conflict of interest.

## Keywords

$CO_2$ methanation, defective boron nitride monolayer, electrochemical mechanisms, first principle calculations, single-atom electrocatalysts

Received: June 28, 2018
Revised: August 13, 2018
Published online: September 10, 2018

[1] N. S. Lewis, D. G. Nocera, *Proc. Natl. Acad. Sci. U. S. A.* **2006**, *103*, 15729.
[2] W. Wang, S. Wang, X. Ma, J. Gong, *Chem. Soc. Rev.* **2011**, *40*, 3703.
[3] J. Wei, Q. Ge, R. Yao, Z. Wen, C. Fang, L. Guo, H. Xu, J. Sun, *Nat. Commun.* **2017**, *8*, 15174.
[4] W. Zhang, Y. Hu, L. Ma, G. Zhu, Y. Wang, X. Xue, R. Chen, S. Yang, Z. Jin, *Adv. Sci.* **2018**, *5*, 1700275.
[5] J. L. Qiao, Y. Liu, F. Hong, J. Zhang, *Chem. Soc. Rev.* **2014**, *43*, 631.
[6] X. Mao, T. A. Hatton, *Ind. Eng. Chem. Res.* **2015**, *54*, 4033.
[7] Q. Lu, J. Rosen, Y. Zhou, G. S. Hutchings, Y. C. Kimmel, J. G. Chen, F. Jiao, *Nat. Commun.* **2014**, *5*, 3242.
[8] X. Hong, K. Chan, C. Tsai, J. K. Nørskov, *ACS Catal.* **2016**, *6*, 4428.
[9] G. Hu, Z. Wu, S. Dai, D.-E. Jiang, *ACS Appl. Mater. Interfaces* **2018**, *10*, 6694.
[10] A. Vasileff, Y. Zheng, S. Z. Qiao, *Adv. Energy Mater.* **2017**, *7*, 1700759.
[11] J. Wu, Y. Huang, W. Ye, Y. Li, *Adv. Sci.* **2017**, *4*, 1700194.
[12] J. Shen, R. Kortlever, R. Kas, Y. Y. Birdja, O. Diaz-Morales, Y. Kwon, I. Ledezma-Yanez, K. J. P. Schouten, G. Mul, M. T. M. Koper, *Nat. Commun.* **2015**, *6*, 8177.
[13] R. Kortlever, J. Shen, K. J. P. Schouten, F. Calle-Vallejo, M. T. M. Koper, *J. Phys. Chem. Lett.* **2015**, *6*, 4073.
[14] C. Peng, G. Reid, H. Wang, P. Hu, *J. Chem. Phys.* **2017**, *147*, 030901.
[15] K. Manthiram, B. J. Beberwyck, A. P. Alivisatos, *J. Am. Chem. Soc.* **2014**, *136*, 13319.
[16] M. Younas, L. L. Kong, M. J. K. Bashir, H. Nadeem, A. Shehzad, S. Sethupathi, *Energy Fuels* **2016**, *30*, 8815.
[17] K. P. Kuhl, T. Hatsukade, E. R. Cave, D. N. Abram, J. Kibsgaard, T. F. Jaramillo, *J. Am. Chem. Soc.* **2014**, *136*, 14107.
[18] D.-H. Lim, J. H. Jo, D. Y. Shin, J. Wilcox, H. C. Hama, S. W. Nam, *Nanoscale* **2014**, *6*, 5087.
[19] A. A. Peterson, J. K. Nørskov, *J. Phys. Chem. Lett.* **2012**, *3*, 251.
[20] Y. Hori, K. Kikuchi, S. Suzuki, *Chem. Lett.* **1985**, *11*, 1695.
[21] A. A. Peterson, F. Abild-Pedersen, F. Studt, J. Rossmeisl, J. K. Nørskov, *Energy Environ. Sci.* **2010**, *3*, 1311.
[22] R. L. Cook, R. C. MacDuff, A. F. Sammells, *J. Electrochem. Soc.* **1988**, *135*, 1320.
[23] W. J. Durand, A. A. Peterson, F. Studt, F. Abild-Pedersen, J. K. Nørskov, *Surf. Sci.* **2011**, *605*, 1354.
[24] R. Michalsky, Y.-J. Zhang, A. J. Medford, A. A. Peterson, *J. Phys. Chem. C* **2014**, *118*, 13026.
[25] S. K. Kim, Y.-J. Zhang, H. Bergstrom, R. Michalsky, A. Peterson, *ACS Catal.* **2016**, *6*, 2003.
[26] N. Li, X. Chen, W.-J. Ong, D. R. MacFarlane, X. Zhao, A. K. Cheetham, C. Sun, *ACS Nano* **2017**, *11*, 10825.
[27] Y. Jiao, Y. Zheng, P. Chen, M. Jaroniec, S.-Z. Qiao, *J. Am. Chem. Soc.* **2017**, *139*, 18093.
[28] H. Xu, D. Cheng, D. Cao, X. C. Zeng, *Nat. Catal.* **2018**, *1*, 339.
[29] B. Qiao, A. Wang, X. Yang, L. F. Allard, Z. Jiang, Y. Cui, J. Liu, J. Li, T. Zhang, *Nat. Chem.* **2011**, *3*, 634.
[30] X.-F. Yang, A. Wang, B. Qiao, J. Li, J. Liu, T. Zhang, *Acc. Chem. Res.* **2013**, *46*, 1740.
[31] H. Zhang, G. Liu, L. Shi, J. Ye, *Adv. Energy Mater.* **2018**, *8*, 1701343.
[32] J. M. Thomas, Z. Saghi, P. L. Gai, *Top. Catal.* **2011**, *54*, 588.
[33] M. Ranocchiari, C. Lothschütz, D. Grolimund, J. A. van Bokhoven, *Proc. R. Soc. A* **2012**, *468*, 1985.
[34] J. Zhao, Z. Chen, *J. Am. Chem. Soc.* **2017**, *139*, 12480.
[35] S. Back, J. Lim, N.-Y. Kim, Y.-H. Kim, Y. Jung, *Chem. Sci.* **2017**, *8*, 1090.
[36] G. Zhu, Y. Li, H. Zhu, H. Su, S. H. Chan, Q. Sun, *ACS Catal.* **2016**, *6*, 6294.
[37] Y. Li, H. Su, S. H. Chan, Q. Sun, *ACS Catal.* **2015**, *5*, 6658.
[38] G. Zhu, Y. Li, H. Zhu, H. Su, S. H. Chan, Q. Sun, *Nano Res.* **2017**, *10*, 1641.
[39] J. K. Nørskov, T. Bligaard, A. Logadottir, J. R. Kitchin, J. G. Chen, S. Pandelov, U. Stimming, *J. Electrochem. Soc.* **2005**, *152*, J23.
[40] G. Kresse, J. Hafner, *Phys. Rev. B* **1994**, *49*, 14251.
[41] G. Kresse, D. Joubert, *Phys. Rev. B* **1999**, *59*, 1758.
[42] G. Kresse, J. Furthmüller, *Phys. Rev. B* **1996**, *54*, 11169.
[43] G. Kresse, J. Furthmüller, *Comput. Mater. Sci.* **1996**, *6*, 15.
[44] J. P. Perdew, K. Burke, M. Ernzerhof, *Phys. Rev. Lett.* **1996**, *77*, 3865.
[45] S. Grimme, *J. Comput. Chem.* **2006**, *27*, 1787.
[46] H. J. Monkhorst, J. D. Pack, *Phys. Rev. B* **1976**, *13*, 5188.